IET Microwaves, Antennas & Propagation

Research Article

IET Journals
The Institution of Engineering and Technology

On-metal UHF-RFID passive tags based on complementary split-ring resonators

ISSN 1751-8725
Received on 14th September 2016
Revised 17th January 2017
Accepted on 9th February 2017
E-First on 10th May 2017
doi: 10.1049/iet-map.2016.0782
www.ietdl.org

Simone Zuffanelli[1] ✉, *Gerard Zamora*[1], *Ferran Paredes*[1], *Pau Aguila*[1], *Ferran Martin*[1], *Jordi Bonache*[1]

[1]*Electronic Engineering Department, Autonomous University of Barcelona, Campus UAB, Bellaterra, Spain*

✉ *E-mail: simone.zuffanelli@uab.cat*

Abstract: The use of complementary split-ring resonators (CSRRs) as radiating elements in low-profile on-metal ultra-high-frequency radio-frequency identification (UHF-RFID) tags is explored in this study. First, the radiation properties of the edge-coupled and the non-bianisotropic (NB-CSRR) versions of the CSRR are studied. The tag design strategy is then discussed in detail. On that basis, a compact ($\lambda_0/7 \times \lambda_0/7$) low-profile (1.27 mm) tag prototype based on the non-bianisotropic version of the CSRR (NB-CSRR) antenna is designed and manufactured to operate in the North-American UHF-RFID band. The experimental results validate the theoretical and simulated behaviour, and exhibit a maximum read range of 6.8 m.

1 Introduction

Radio-frequency identification (RFID) is a family of technologies which allow identifying objects by using radio waves. To this end, each item is equipped with a device (RFID tag) which stores specific information (generally, an electronic product code, or EPC) and is able to broadcast such information upon an incoming query from a reading device (RFID reader). In the last years, the progressive reduction of the tag cost resulted in a widespread of RFID technology, and the projections indicate further growth in the next years [1]. Among the typical applications of this technology, access control (e.g. electronic toll collection), smart inventory and item tracking are already well established, while other retail-related applications (e.g. smart shelves, automatic payment) are expected for the near future [1].

Passive tags operating in the ultra-high-frequency RFID (UHF-RFID) frequency band (860–960 MHz [2]) have become widely available on the market, since they offer high reading distances, small dimensions and low cost, and do not need batteries to operate. In these tags, an antenna (usually a printed planar antenna) is connected to an integrated circuit (RFID ASIC) which implements the transponder, and contains the specific information regarding the object. When the query signal radiated by the reader is received by the tag antenna, it is delivered to the ASIC, which is able to extract the RF energy to feed its circuitry and generates a series of modulated reflections containing the requested information back to the reader. The reading distance (read range) is in the order of 5–12 m, depending on the tag performance (i.e. antenna efficiency, impedance matching and ASIC sensitivity), the materials of the tagged item and the environmental conditions.

Metamaterials and metamaterial-inspired resonators [e.g. split-ring resonators (SRRs)] have been recently employed to the design of RFID devices, and showed they can improve the size, the impedance matching and the radiation properties of reader [3–5] and tag [6–10] antennas. Also, their complementary counterparts, especially the complementary split-ring resonator (CSRR) and other structures derived from it, were used to obtain compact RFID tags, as follows. In [11, 12], modified CSRRs were connected in series to lower the resonant frequency of dipole tag antennas, whereas a CSRR-based inter-layer is used in [13] to shrink the size of a fractal patch antenna for on-metal RFID applications. Nevertheless, the use of complementary resonators as standalone radiating elements in UHF-RFID tags has not been reported. Due to the dipole moments generated at resonance, which satisfy boundary conditions imposed by metallic surfaces, this kind of particle is especially suitable for on-metal tags with very low profile, which still represent a major challenge in RFID technology. It is worth to mention that most of the on-metal UHF-RFID tags found in the literature are based on patch antennas or derived structures [14], and therefore the study of alternative designs is especially interesting.

The paper is organised as follows. First, the radiation properties of CSRRs on metallic surfaces are discussed in Section 2. The RFID tag design strategy is then presented in Section 3, and applied to the design and simulation of a tag prototype. The experimental measurements of the fabricated tag are detailed in Section 4, where a comparison with the state-of-the-art solutions is also provided.

2 Radiation properties of CSRRs over metallic surfaces

The topologies of the edge-coupled (EC-SRR) and the non-bianisotropic (NB-SRR) SRRs are depicted in Fig. 1. The radiation resistance of the EC-SRR around the first and second self-resonances has been recently calculated analytically as a function of the particle mean radius r_0 [10, 15], defined as the arithmetic mean of the inner and outer ring radii. These results also hold true for the NB-SRR, since it presents approximately the same current profile at both the first and second resonances [16]. Furthermore, these results can be directly extended to the case of an ideal (i.e. unbounded and lossless) CSRR, by applying duality [17]. From the well-known Booker relations [18], the radiation conductance around the first and second resonances can be approximated by

$$G_{\mathrm{rad},1} \simeq \frac{32}{3}\frac{\pi^5}{Z_0}\left(\frac{r_0}{\lambda_0}\right)^4 \tag{1}$$

$$G_{\mathrm{rad},2} \simeq \frac{512}{27}\frac{\pi}{Z_0}\left(\frac{r_0}{\lambda_0}\right)^2, \tag{2}$$

where Z_0 is the impedance of free space and λ_0 is the free-space wavelength at the operation frequency. Duality suggests that radiation is mainly provided by an axial electric dipole moment and a tangential magnetic dipole moment at the first and second resonances, respectively. In the case of the EC-CSRR, further contribution to radiation arises from the bianisotropy of the structure, which generates a small cross-polar radiation, but its effect on the radiation conductance can be neglected [10, 15]. Regarding the tangential magnetic dipole arising at the second resonance, it is oriented along the y-axis in the case of the EC-

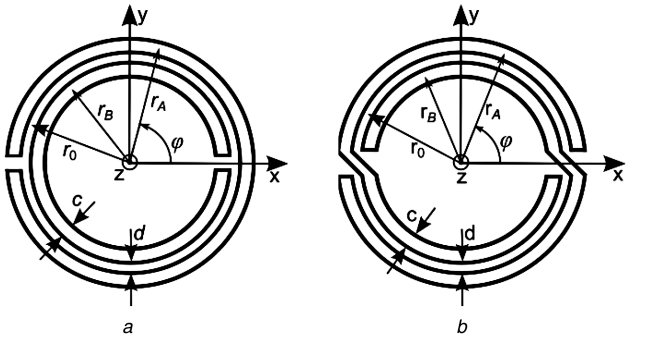

Fig. 1 *Topology of the*
(a) Edge-coupled (EC-SRR) SRR, ***(b)*** Non-bianisitropic (NB-SRR) SRR

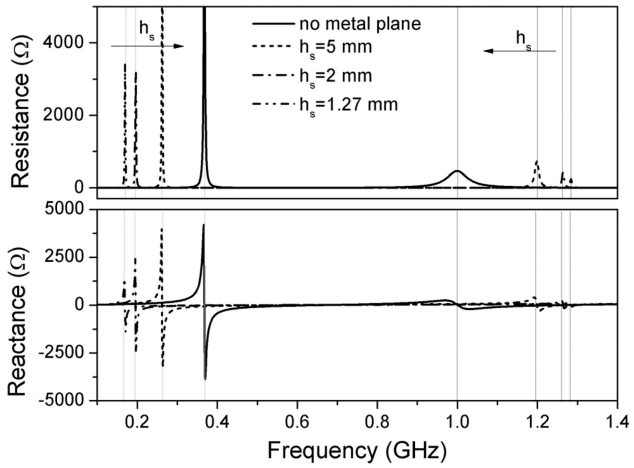

Fig. 2 *Simulated input impedance of a lossy (etched on a squared copper layer with side length L = 75 mm) EC-CSRR placed at different distances h_S over an infinite ground plane (first resonances are marked in light grey, second resonances in dark grey), and driven at the external ring centre. The dimensions are r_0 = 35.25 mm, c = 2 mm and d = 0.5 mm*

Table 1 Simulated values for the first and second resonant frequencies of the CSRR mounted over an ideal ground plane

Distance from ground	f_1, GHz	f_2, GHz	η_{rad1}, %	η_{rad2}, %
no ground	0.37	1	45	98
h_S = 5 mm	0.26	1.2	6	77
h_S = 2 mm	0.2	1.26	2	46
h_S = 1.27 mm	0.17	1.28	<1	30

CSRR [15], as a result of the particle symmetry plane. Conversely, in the NB-CSRR the inner part of the rings is shorter than the outer part, so that the dipole axis is expected to be slightly rotated clockwise, and the rotation angle depends on the geometry of the particle.

Let us now consider the more complex case of a limited and lossy screen, placed at distance h_s over a metallic surface. From image theory [19], the structure behaves in the upper half-space (delimited by the ground plane) as a system composed of two parallel complementary screens, with a separation distance $2h_s$, which presents anti-symmetrical current distribution. Hence, a system of two coupled CSRRs separated by an electric wall is obtained. Coupled resonators theory [20] states that, in this case, the fundamental resonance frequency is lowered (as compared with the uncoupled resonator) when the coupling between resonators is electric, while it is raised when the coupling is magnetic. Since the CSRR generates a strong axial electric dipole moment at the first resonance, coupling is electric, and the first resonance is lowered. Contrarily, the second resonance is lowered by the ground plane because the CSRR exhibits a magnetic behaviour and therefore is magnetically coupled to its image. Additionally, the ground plane reduces the antenna efficiency in both cases, since it introduces several loss mechanisms. First, being the radiation restricted to a half-space, the radiation conductance G_{rad} is halved [18], with respect to an ideal CSRR. Moreover, the currents on the CSRR screen increase (for a given voltage applied across the slot) due to the additional capacitance introduced by the ground plane, which involves an overall increase of the ohmic losses. Finally, the currents induced on the ground plane, or the presence of a dielectric substrate, also contribute to increase losses and reduce efficiency.

The abovementioned behaviour was validated by means of electromagnetic (EM) simulations (CST Microwave Studio), which quantified the input impedance (see Fig. 2), the resonant frequencies and the radiation efficiency (Table 1) of a CSRR etched on a squared copper screen placed at several distances h_s on a metallic plane, and driven by a differential port connected at the centre of the external ring. In order to avoid radiation from the patch formed by the finite screen and the underlying ground plane, the four sides of the screen containing the CSRR were short-circuited to ground by means of vias. The results suggest that, even for very small distances from the metal, the radiation efficiency at the second resonance maintains relatively high values (i.e. η_{rad} = 30% for h_s = 1.27 mm).

The simulations did not consider the presence of any dielectric substrate. Obviously, a substrate is necessary in practice, as a support for the top metal layer. The dielectric constant of the substrate can thus be chosen in order to properly reduce the tag size, which is necessary when working at the second resonance because the ground plane causes significant increase in dimensions (roughly 100 mm × 100 mm, for h_s = 1.27 mm, which is unpractical for most applications). However, a trade-off arises between final tag size and performance, as already mentioned.

3 Tag design

3.1 Design strategy

In this section, the design of a low-profile on-metal UHF-RFID tag employing the NB-CSRR antenna at its second resonance is detailed.

The tag layout is depicted in Fig. 3. In this proof of concept, we prioritised size reduction, while maintaining a reasonable read range. Hence, a high-permittivity substrate was chosen, namely the Rogers RO3010 (with relative permittivity ε_r = 10.2, loss tangent tanδ = 0.0023 and thickness h_s = 1.27 mm). The NB-CSRR was chosen due to its simpler radiation diagram, which is the result of a single radiating dipole moment, and exhibits very low values (ideally zero) of cross-polarisation.

Let us now present the impedance matching strategy between the ASIC and the antenna, which is a critical aspect of passive UHF-RFID tag design. The input impedance of UHF-RFID ASICs is usually modelled by a parallel RC circuit [21], while the antenna can be modelled around resonance by a parallel RLC circuit [22], as shown in Fig. 3*c*. Due to the very small electrical size of the antenna and to the presence of a nearby ground plane, the radiation quality factor of the system is expected to be high, which leads to high susceptance slopes around resonance [22]. Therefore, a resonance between the antenna and the ASIC is expected just below the CSRR resonance, in the resonator inductive region. At that frequency, the matching level depends on the ratio between G_c and G_a, which varies as a function of the position φ_p of the input port along the slot, as already reported in the case of moving the input port along the SRR ring [10]. Concretely, the NB-CSRR input conductance is raised when moving the port towards the ends of the slot, so that it is possible to obtain good impedance matching without introducing any a matching network. Obviously, the antenna conductance at the centre of the NB-CSRR (which is the lowest value) must be lower than the ASIC conductance to ensure the existence of a position which provides good impedance matching.

To locate the second resonance of the particle to the desired frequency, there are mainly three parameters to take into account.

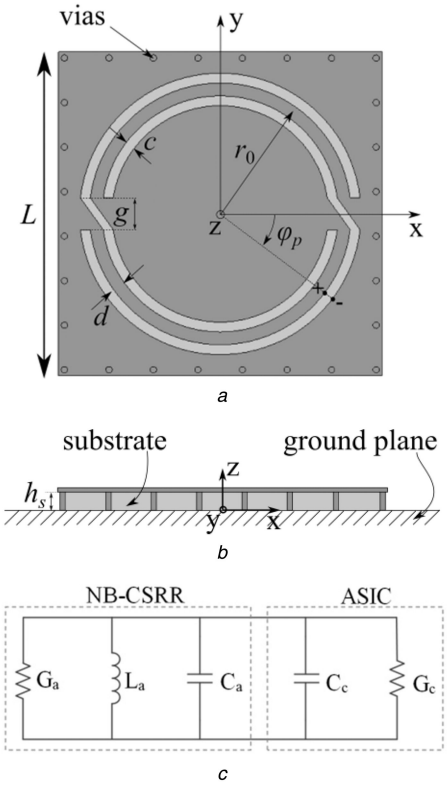

Fig. 3 *Proposed tag layout*

(a) Top view, ***(b)*** Side view (not to scale), ***(c)*** Tag circuit model around resonance. Copper is represented in dark grey, dielectric in light grey. The angle φ_p indicates the position of the excitation port

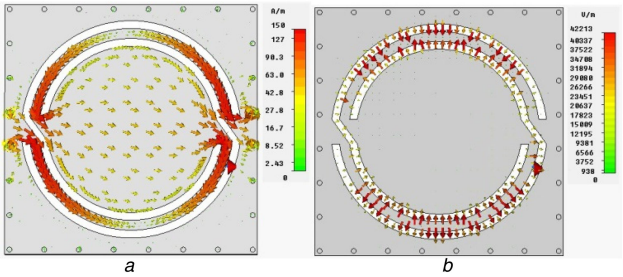

Fig. 4 *Simulated*

(a) Surface current density on the screen, ***(b)*** Electric field inside the slot at the second NB-CSRR resonance. The red cone indicates the excitation port

The first is, obviously, the particle average radius r_0, which controls the overall lateral dimensions of the particle. Then, the separation d of the slots, which controls the coupling between the resonators, can be used as a design parameter since it offers an additional degree of freedom on the tag dimensions. It is well known that increasing the coupling between the resonators the frequency split of the first and second resonances increases, that is, the first resonance is lowered and the second is raised in frequency. Lastly, the thickness h_s of the dielectric also affects the resonance frequencies, since it is the distance between the particle and the metal plane (see Section 2).

3.2 Final layout and simulation results

As a proof of concept, a tag working at the North-American UHF-RFID band (902–928 MHz, centred at $f_0 = 915$ MHz), and based on the Alien Higgs 3 chip transponder (SOT-323 packaged, with power sensitivity $P_{th} = -17$ dBm and input impedance modelled by $G_c = 0.66$ mS and $C_c = 0.9$ pF), was designed with the aid of EM simulations (CST Microwave Studio), as follows.

First, the CSRR dimensions were adjusted to locate the second resonance at 920 MHz, i.e. closely above to the operating frequency, where resonance is expected to occur (see Section 3.1).

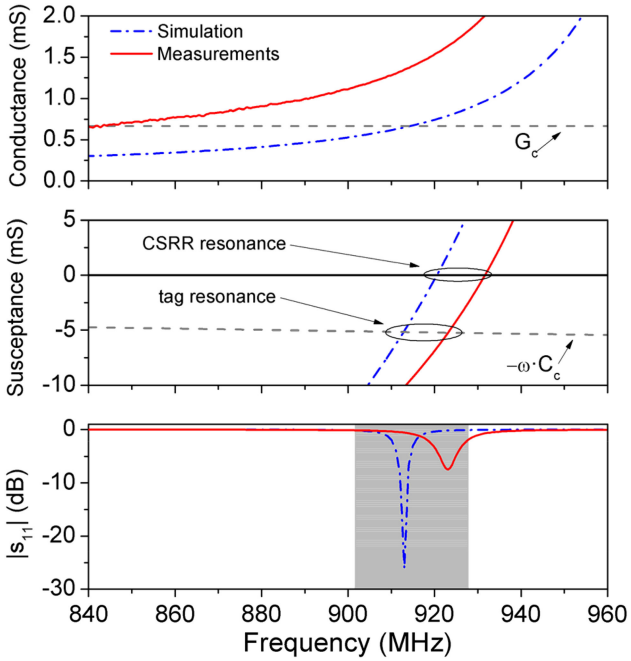

Fig. 5 *Input admittance and reflection coefficient of the tag prototype. The reflection coefficient was measured for a differential 100 Ω port and renormalised to the impedance of the RFID ASIC. The North-American UHF-RFID band is depicted in grey*

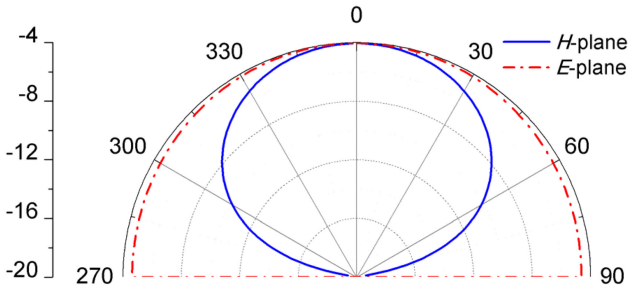

Fig. 6 *Simulated radiation pattern of the tag in the H-plane (φ = 60°) and E-plane (φ = −30°) at the tag resonance*

The following dimensions were found: $L = 45$ mm, $r_0 = 17.3$ mm, $c = 1.4$ mm, $d = 1.8$ mm and $g = 4.5$ mm. Then, the port position was swept until reaching proper impedance matching, which was provided at the position $\varphi_p = -20°$.

The simulation results, in terms of currents on the screen and electric field inside the slot, are shown in Fig. 4. From the electric field distribution it can be deduced that the equivalent magnetic current in the two rings flows in opposite directions, as expected at the second resonance of the NB-CSRR [16]. However, due to the increase of the resonance frequency caused by the vicinity of the metal plane, the magnetic current presents two maxima, located at roughly ±90°. The simulated input admittance and reflection coefficient, depicted in Fig. 5, shows good impedance matching (−25 dB) at 913 MHz, where the inductive susceptance of the antenna compensates the capacitive behaviour of the ASIC. Finally, the radiation pattern, depicted in Fig. 6, agrees with that of a tangential magnetic dipole moment oriented along the direction $\varphi = 60°$, in concordance with theory (see previous section).

The radiation efficiency provided by the simulator is $\eta_{rad} = 12\%$ (ohmic losses on the copper screen account for 62% of the total losses, versus 38% of dielectric losses), resulting in a maximum gain of $G_r = -4$ dB (at $\theta = 0°$). Based on this value, it is possible to predict the maximum tag read range, which is given by [23]

$$\mathrm{RR} = \frac{\lambda_0}{4\pi}\sqrt{\frac{\mathrm{EIRP} \cdot G_r \cdot \tau}{P_{th}}}, \tag{3}$$

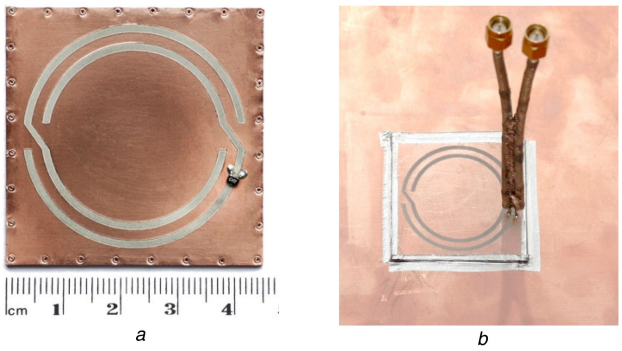

Fig. 7 *Fabricated*
(a) Tag prototype, ***(b)*** Measurement assembly of the antenna input impedance (mounted on the ground plane)

where EIRP is the equivalent isotropic radiated power of the RFID reader, P_{th} is the ASIC read sensitivity and $\tau = (1 - |s_{11}|^2)$ is the power transmission coefficient. By assuming EIRP = 4 W, which is the maximum allowed value in the North-American UHF-RFID band [2], and $\tau \simeq 1$, the predicted read range with Alien Higgs 3 reaches RR = 7.4 m.

4 Fabrication and measurements

To validate the theoretical and simulated results, the layout described in the previous section was fabricated (Fig. 7*a*) by means of a printed circuit board (PCB) drilling machine (*LPKF-H100*). All the measurements were performed with the tag prototype attached to a 20 cm × 30 cm ground plane by means of adhesive tape. The measurements presented below refer to a corrected version of the tag, where the value of r_0 was scaled (1% larger) to correct a frequency shift (15 MHz) detected in the experimental read range. Such a small frequency shift, commonly encountered when fabricating UHF-RFID tags, can be attributed to the fabrication tolerances, and to the simulation accuracies as well. In this case, due to the presence of the metal layer, the tag response also exhibits a strong dependence upon the substrate thickness, which adds further contribution to the frequency shift as compared with a general purpose tag.

4.1 Measurement setup

An Agilent *N5221A* two-port network analyser was used to measure the antenna impedance. To properly excite the antenna, a test fixture based on two semi-rigid coaxial cables soldered together was employed (Fig. 7*b*). Then, the measured scattering parameters were used to evaluate the differential input impedance, by using the method reported in [24].

The tag read range was measured in a controlled environment, namely a *Wavecontrol WaveCell* transverse electromagnetic mode (TEM) cell excited by a 50 Ω coaxial cable connected to a vector signal generator (Agilent *N5182A*), which is able to generate RFID frames at different power levels. The signal backscattered from the TEM cell was sent to an *Agilent N9020A* signal analyser by means of a circulator, where the tag responses were read. The tag, mounted on a 20 × 30 cm ground plane, was held inside the TEM cell by using a foam support and properly oriented along its main radiation lobe. The tag read range was then evaluated by measuring the minimum interrogation signal power (P_{min}) necessary to obtain a successful response, and then probing the electric field strength E_{rms} at the tag position by means of an electric field probe (*Wavecontrol EFCube*). Considering that the average power density S associated to a plane wave is given by

$$S = \frac{E_{\text{rms}}^2}{Z_0}, \tag{4}$$

and that the power density at a given distance from a transmitting antenna is provided by

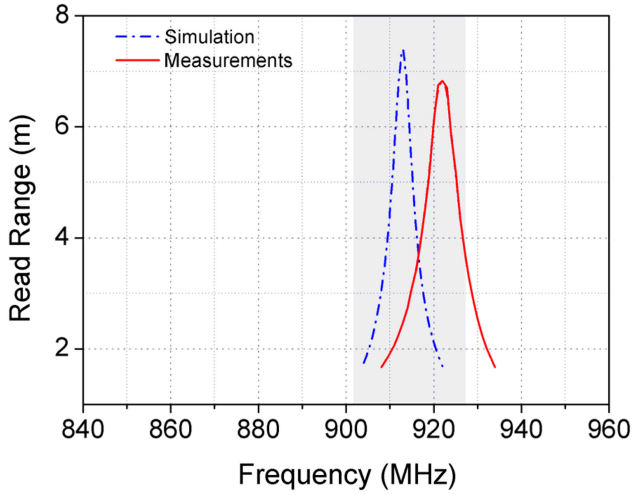

Fig. 8 *Simulated and experimental tag read range. The North-American UHF-RFID band is marked in grey*

$$S = \frac{P_{\text{t}} G_{\text{t}}}{4\pi r^2} = \frac{\text{EIRP}}{4\pi r^2} \tag{5}$$

(where P_{t} is the total transmission power, G_{t} is the antenna gain and r is the distance from the antenna), the read range RR can be obtained by (4) and (5). The result is

$$\text{RR} = \frac{\sqrt{30\text{EIRP}}}{E_{\text{rms}}}. \tag{6}$$

To obtain the curve of the tag read range, the process was then iterated for each frequency of interest (e.g. at 1 MHz steps).

4.2 Experimental results and discussion

The antenna input impedance, depicted in Fig. 5, was measured at the port position $\varphi_p = -20°$ (the RFID ASIC was not mounted at this stage). Reasonable agreement with the simulated values is obtained, though a residual frequency shift is observed (the tag resonates at $f_0 = 923$ MHz), and the input conductance at resonance (1.6 mS) is higher than the simulated value (0.66 mS). By renormalising the scattering parameters to the impedance of the RFID ASIC, a minimum reflection level of −8 dB (consequently, $\tau = 0.84$) is obtained (Fig. 5), which involves a 8% reduction of the peak read range, as compared with conjugate matching. The experimental read range is depicted in Fig. 8. The tag response is centred at the frequency $f_0 = 923$ MHz, and the maximum read range is 6.8 m, which is in very good agreement with simulations when the mismatch correction mentioned above is applied.

In light of its novelty and performance, the proposed approach is an interesting alternative to the commonly employed patch-derived structures. In fact, as can be seen in Table 2, the presented tag is competitive against the state of the art of very-low-profile on-metal UHF-RFID tags. However, further research on the subject is needed to avoid using high-permittivity substrates, and/or to further reduce the tag thickness or lateral dimensions.

5 Conclusion

The radiation properties of CSRRs placed at very small distances from a metallic plane have been studied in this work. Based on duality, qualitative predictions of the particle behaviour were provided and then validated by EM simulations, which suggested that the CSRR presents acceptable radiation efficiency near its second resonant frequency even for very low distances from the ground plane. Based on these results, the design strategy of a passive UHF-RFID tag based on such antenna was then presented, where it was shown that good impedance matching between the RFID ASIC and the NB-CSRR antenna could be obtained without the need of any matching network.

Table 2 Comparison with state-of-the-art low-profile on-metal tags

Ref.	Thickness, mm	Size, mm	Metal layers	Substrate	RR_{norm}[a], m
[13]	3.2	37 × 18	2	FR4	1.4
[25]	2.4	26 × 14	2	FR4, PTFE	7
[26]	1.6	40 × 80	1	FR4	6.7
[27]	1.6	42 × 42	1	Rogers *RT/duroid*	4.6
[28]	1.5	32 × 32	1	Composite ($BaTiO_3$ + PDMS)	2.1
This	1.27	45 × 45	1	Rogers (*RO3010*)	6.8
[29]	0.8	60 × 90	1	FR4	5.2

[a] RR_{norm} is the tag read range referred to a chip sensitivity of $P_{th} = -17$ dBm.

As a proof of concept, a compact ($\simeq\lambda_0/7 \times \lambda_0/7$) and low-profile (1.27 mm) tag based on the NB-CSRR antenna was designed and fabricated to operate on metal in the North-American UHF-RFID band. The experimental read range is in good agreement with simulations, and reaches 6.8 m, thus validating the suitability and competitiveness of the proposed approach for building on-metal tags with reduced thickness.

6 Acknowledgments

This work was supported by MINECO-Spain (project TEC2013-40600-R COM-SEN-RFID), FEDER funds and Generalitat de Catalunya (project 2014SGR-157). Ferran Martín is in debt to ICREA for supporting his work and by awarding him with an ICREA Academia Award.

7 References

[1] Das, R., Harrop, P.: '*RFID forecasts, players and opportunities 2009–2019*' (IDTechEX, 2009)

[2] '*Regulatory status for using RFID in the EPC Gen 2 band (860 to 960 MHz) of the UHF spectrum*' (GS1 EPCglobal, 2013)

[3] Braaten, B.D., Roy, S., Nariyal, S., *et al.*: 'A metamaterial-based series connected rectangular patch antenna array for UHF RFID Readers'. 6th European Conf. on Antennas and Propagation (EuCAP), Prague, March 2012, pp. 3164–3167

[4] Smierzchalski, M., Collardey, S., Mahdjoubi, K.: 'A novel metamaterial-based RFID antenna with efficient of operating distance'. 6th European Conf. on Antennas and Propagation (EuCAP), Prague, March 2012, pp. 3038–3041

[5] Jung, Y.K., Lee, B.: 'Dual-band circularly polarized microstrip RFID reader antenna using metamaterial branch-line coupler', *IEEE Trans. Antennas Propag.*, 2012, **60**, (2), pp. 786–791

[6] Braaten, B.D., Reich, M., Glower, J.: 'A compact meander-line UHF RFID tag antenna loaded with elements found in right/left-handed coplanar waveguide structures', *IEEE Antennas Wirel. Propag. Lett.*, 2009, **8**, pp. 1158–1161

[7] Paredes, F., Zamora, G., Martin, F., *et al.*: 'Miniaturization of RFID tag by means of an electrically small resonator'. IEEE Int. Conf. on Wireless Information Technology and Systems (ICWITS), Honolulu, Hawaii, September 2010, pp. 1–4

[8] Paredes, F., Zamora, G., Herraiz-Martínez, F.J., *et al.*: 'Dual-band UHF-RFID tags based on meander-line antennas loaded with spiral resonators', *IEEE Antennas Wirel. Propag. Lett.*, 2011, **10**, pp. 768–771

[9] Lim, S.H., Oh, Y.C., Lim, H., *et al.*: 'Analysis and design of a UHF RFID tag antenna with a split ring resonator'. Int. Workshop on Antenna Technology: Small Antennas and Novel Metamaterials, Chiba, Japan, March 2008, pp. 446–449

[10] Zuffanelli, S., Zamora, G., Aguila, P., *et al.*: 'Analysis of the split ring resonator (SRR) antenna applied to passive UHF-RFID tag design', *IEEE Trans. Antennas Propag.*, 2015, **64**, (3), pp. 856–864

[11] Braaten, B.D.: 'A novel compact UHF RFID tag antenna designed with series connected open complementary split ring resonator (OCSRR) particles', *IEEE Trans. Antennas Propag.*, 2010, **58**, (11), pp. 3728–3733

[12] Braaten, B.D., Aziz, M.: 'Using meander open complementary split ring resonator (MOCSRR) particles to design a compact UHF RFID tag antenna', *IEEE Antennas Wirel. Propag. Lett.*, 2010, **9**, pp. 1037–1040

[13] Jalal, A.S.A., Ismail, A., Alhawari, A.R.H., *et al.*: 'Metal mount fractal RFID tag antenna with complementary split ring resonators'. IEEE Int. Conf. on RFID Technologies and Application (RIFD-TA), Johor Bahru, Malaysia, September 2013, pp. 1–5

[14] Bjorninen, T., Sydanheimo, L., Ukkonen, L., *et al.*: 'Advances in antenna designs for UHF RFID tags mountable on conductive items', *IEEE Antennas Propag. Mag.*, 2014, **56**, pp. 79–103

[15] Zuffanelli, S., Zamora, G., Aguilà, P., *et al.*: 'On the radiation properties of split-ring resonators (SRRs) at the second resonance', *IEEE Trans. Microw. Theory Tech.*, 2015, **63**, (7), pp. 2133–2141

[16] Garcia, J., Martin, F., Baena, J.D., *et al.*: 'On the resonances and polarizabilities of split ring resonators', *J. Appl. Phys.*, 2005, **98**, (3), pp. 33103–33103-9

[17] Falcone, F., Lopetegi, T., Baena, J.D., *et al.*: 'Effective negative-ε stopband microstrip lines based on complementary split ring resonators', *IEEE Microw. Compon. Lett.*, 2004, **14**, (6), pp. 280–282

[18] Booker, H.G.: 'Slot aerials and their relation to complementary wire aerials (Babinet's principle)', *J. Inst. Electr. Eng. IIIA, Radiolocation*, 1946, **93**, pp. 620–626

[19] Balanis, C.A.: '*Antenna theory: analysis and design*' (John Wiley, 2005)

[20] Hong, J.S., Lancaster, M.J.: '*Microstrip filters for RF/microwave applications*' (Wiley, 2001)

[21] De Vita, G., Iannaccone, G.: 'Design criteria for the RF section of UHF and microwave passive RFID transponders', *IEEE Trans. Microw. Theory Tech.*, 2005, **53**, (9), pp. 2978–2990

[22] Yaghjian, A.D., Best, S.R.: 'Impedance, bandwidth and Q of antennas', *IEEE Trans. Antennas Propag.*, 2005, **53**, (4), pp. 1298–1324

[23] Rao, K.V.S., Nikitin, P.V., Lam, S.F.: 'Antenna design for UHF RFID tags: a review and a practical application', *IEEE Trans. Antennas Propag.*, 2005, **53**, (12), pp. 3870–3876

[24] Qing, X., Goh, C.K., Chen, Z.N.: 'Impedance characterization of RFID tag antennas and application in tag co-design', *IEEE Trans. Microw. Theory Tech.*, 2009, **57**, (5), pp. 1268–1274

[25] Zhang, J., Long, Y.: 'A novel metal-mountable electrically small antenna for RFID tag applications with practical guidelines for the antenna design', *IEEE Trans. Antennas Propag.*, 2014, **62**, (11), pp. 5820–5829

[26] Lee, B., Yu, B.: 'Compact structure of UHF band RFID tag antenna mountable on metallic objects', *Microw. Opt. Technol. Lett.*, 2008, **50**, (1), pp. 232–234

[27] Koskinen, T.V., Rajagopalan, H., Rahmat-Samii, Y.: 'A thin multi-slotted dual patch UHF-band metal-mountable RFID tag antenna', *Microw. Opt. Technol. Lett.*, 2011, **53**, (1), pp. 40–47

[28] Babar, A.A., Björninen, T., Bhagavati, V., *et al.*: 'Small and flexible metal mountable passive UHF RFID tag on high-dielectric polymer-ceramic composite substrate', *IEEE Antennas Wirel. Propag. Lett.*, 2012, **11**, pp. 1319–1322

[29] Chen, H.D., Tsao, Y.H., Kuo, C.Y.: 'Low-profile radio frequency identification tag antenna using a trapezoid patch mountable on metallic surfaces', *Microw. Opt. Technol. Lett.*, 2010, **52**, pp. 1697–1700